THE ASTROPHYSICAL JOURNAL, 272:456–472, 1983 September 15

GLOBULAR CLUSTER SYSTEMS IN THE HYDRA I ELLIPTICAL GALAXIES. II.

WILLIAM E. HARRIS[1]
Department of Physics, McMaster University, Canada
MALCOLM G. SMITH[1]
Royal Observatory, Edinburgh, Scotland
AND
ERIC S. MYRA
Department of Physics, McMaster University, Canada
Received 1982 September 3; accepted 1983 March 2

ABSTRACT

We have carried out a deep ($B_{\mathrm{lim}} \approx 24.5$) photometric survey around NGC 3311, the giant central galaxy of the Hydra I (A1060) Cluster, to investigate the characteristics of its globular cluster system. Measurements of the images in a 7'.4 square field centered on NGC 3309/3311, compared with a "background" field $\sim 15'$ away, have been used to derive the following results: (*a*) NGC 3311 is surrounded by an extensive and extremely populous cluster system, with an approximate projected space density dependence $\sigma(r) \sim r^{-1.4}$ that is similar to the light intensity distribution of the galaxy itself. (*b*) Various numerical tests on our data suggest that the other two giant elliptical galaxies in the Hydra core region, NGC 3308 and 3309, contain no detectable cluster populations down to $B \sim 24$, and thus that NGC 3311 completely dominates Hydra in this respect. (*c*) The NGC 3311 globular clusters appear in detectable numbers for $B_J > 22$, increasing steadily to the survey limit. Their distribution in apparent magnitude is satisfactorily matched by the standard Virgo/Local Group luminosity function for globular clusters if Hydra is placed (2.0 ± 1.0) mag farther away than Virgo, corresponding to d(Hydra) ≈ 35 Mpc if d(Virgo) ≈ 15 Mpc. (*d*) NGC 3311 represents the first additional example of a "supergiant," or anomalously populous, globular cluster system, similar to the system in the Virgo giant elliptical galaxy M87. For any reasonable distance estimate the cluster specific frequency (number of clusters per unit galaxy luminosity) is $S(3311) \gtrsim 20$, which is $\gtrsim 3$ times the normal value for globular cluster systems in elliptical galaxies generally. We discuss the possible connections between the M87 and NGC 3311 situations, with the tentative suggestion that their exceptional cluster populations may have been acquired at birth rather than in subsequent evolution.

Subject headings: clusters: globular — galaxies: clusters of — galaxies: individual — galaxies: stellar content

I. INTRODUCTION

The Hydra I cluster of galaxies (A1060) is a moderately rich system whose central region is dominated by the three giant elliptical galaxies NGC 3308, 3309, and 3311. Smith and Weedman (1976, hereafter Paper I) carried out photographic photometry of the stellar images in a small region of the Hydra center and argued that NGC 3311, in particular, appeared to contain a detectable population of globular clusters which began to appear in larger numbers near $B \approx 24$. At a mean redshift $V_0 \approx 3400$ km s^{-1} (Richter, Materne, and Huchtmeier 1982), Hydra therefore contains the most distant galaxies within which globular clusters are currently known (cf. Harris and Racine 1979, hereafter HR).

Study of the basic characteristics of globular cluster systems in elliptical galaxies (their total numbers, spatial distribution around the parent galaxy, and distribution in magnitude) has numerous applications toward understanding potential evolutionary differences between the globular clusters and the galaxy halo itself, the many possible effects of parent-galaxy environment, and the calibration of the extragalactic distance scale (for more complete discussions see, e.g., Hanes 1979; HR; Strom *et al.* 1981; Forte, Strom, and Strom 1981; Harris and van den Bergh 1981). To date, globular cluster systems have been detected in $\lesssim 20$ large elliptical galaxies in Virgo and nearby smaller groups ($500 \lesssim V_0 \lesssim 1500$ km s^{-1}; cf. HR; Hanes 1977; Harris and van den Bergh 1981), but significantly more distant systems have so far remained largely unexplored territory.

[1]Visiting Astronomer, Kitt Peak National Observatory, which is operated by the Association of Universities for Research in Astronomy, Inc., under contract to the National Science Foundation.

An additional point of interest for elliptical galaxies in a substantial cluster such as Hydra is to investigate whether any of them might turn out to be an analog of M87 in Virgo, with its enormously (and anomalously) large globular cluster population. Ideas have been proposed to relate the size of the M87 system with its dynamical position at the center of the Virgo Cluster, or its evolutionary history at critical early epochs (e.g., van den Bergh 1977*a*; HR; Harris 1981; Forte, Martinez, and Muzzio 1982); these ideas are likely to remain as mere speculation unless and until other examples similar to the M87 system can be found.

Smith and Weedman (Paper I) were able to analyze the faint images near NGC 3311 itself over only a small portion of the original plate material essentially because of the limited computer software then available for handling large numbers of faint photographic images. Since then, rapid progress in image-processing capabilities has now enabled photometry of thousands of images on deep photographic plates to be routinely carried out. We have therefore been able to continue and extend the study of the Hydra elliptical galaxies started in Paper I.

The majority of our results depend on analysis of a single deep plate (CPF 994), one of an original set of six prime-focus exposures taken by M. G. S at the Cerro Tololo Inter-American Observatory 4 m telescope in 1975 (all on baked IIIa-J + GG385). Plate 994 is clearly the deepest of the entire set and reveals a plainly visible concentration of faint starlike images around the central pair of galaxies (NGC 3309/3311). The seeing disk on plate 994 (the FWHM of profiles fitted to the fainter images) is $1''.2$, and its faintest measured images reach $B > 24.5$. Although it should prove possible to obtain even fainter photometry in selected areas, with (for example) CCD detectors, deeper photographic observations covering the wide field necessary to measure the global properties of the Hydra globular cluster systems will require quite exceptional observing conditions. Rather than obtaining new plate material, we therefore attempted to subject CPF 994 to a more comprehensive analysis than was possible in Paper I.

II. MEASUREMENTS AND CALIBRATION

During 1980 July we scanned plate 994 with the PDS microdensitometer at Kitt Peak National Observatory. The scans were made in four separate square regions of identical size, as illustrated in Figure 1: a "core" field containing the NGC 3309/3311 pair, in which the faint excess images are most evident, flanked by three "background" fields (B1, B2, B3). The PDS was operated with a 12 micron spot size, with each scanned region being 2000×2000 pixels (or $\sim 7'.4$ on a side). Following density-to-intensity conversion of the scans, our analysis of the individual areas was generally similar to the approach described by Strom *et al.* (1981) for the M87 cluster system. The first step was to eliminate the large-scale background light gradient from the central large elliptical galaxies themselves: in brief, a "blurred," low-resolution map of each scan was constructed from the original frame by a combination of block averaging and median filtering, to eliminate all the small-scale structure (i.e., images $\lesssim 10''$ in size). Subtracting this blurred picture from the original then yielded a frame containing essentially nothing but the small-scale images superposed on a "flat" sky background of mean intensity ~ 0. (The batch routine SKYFLAT was used for this purpose; more detailed descriptions are provided by Strom *et al.* 1981 and the program documentation from KPNO.)

Figure 2 illustrates the effectiveness of the sky gradient removal in the crucial core field (compare this with Fig. 2 of Strom *et al.*). Except for the saturated centers of the large-galaxy images, the "flattened" frame provides a much more manageable region than the original picture in which to detect images unambiguously and carry out conventional stellar photometry.

On each flattened field, we completed the photometry in two separate (and later complementary) ways. The first was to use the automated PFIND routine (part of the AUTOPHOT package; see Wells 1980), which detects all pixels above a specified threshold intensity and collects them into separate images. The intensity-weighted image center positions and their "isophotal" magnitudes (i.e., the total intensity of all detected pixels above threshold) are then calculated. We adopted a pixel detection threshold of 2.5 times the rms scatter of the sky background. No distinction was made at this stage between "stellar" images and nonstellar ones; the primary aim of this approach was only to produce a complete sample of data down to a clearly specified limit.

Our second approach was to measure each field manually and interactively with the IPPS Comtal terminal at KPNO. On the video display of each section of the field, the contrast and range of the gray-scale mapping can be readily adjusted at the terminal, so that the structures of the images in each frame can be quickly inspected. The nonstellar images (i.e., faint background galaxies, plate flaws, etc.) with sizes $\gtrsim 1''.5$–$2''.0$ were selected out, and all remaining (starlike) images visible to the eye were then measured with a concentric-aperture photometry routine (2CAP; see Strom *et al.* 1981 and Wells 1980). The synthetic aperture sizes we used consisted of a central star circle of diameter 14 pixels ($= 3''.1$) and a surrounding sky annulus with inner and outer radii of 19 and 29 pixels ($4''.2$ and $6''.5$). The main advantage of this approach (aside from facilitating some important visual control over our results) was to produce a data sample in which a large fraction of the contaminating nonstellar images had been reliably removed; its principal *disadvantage* was the subjective and hence uncertain magnitude completeness limit.

The manually obtained 2CAP magnitudes (denoted m_a) were also employed to calibrate the isophotal

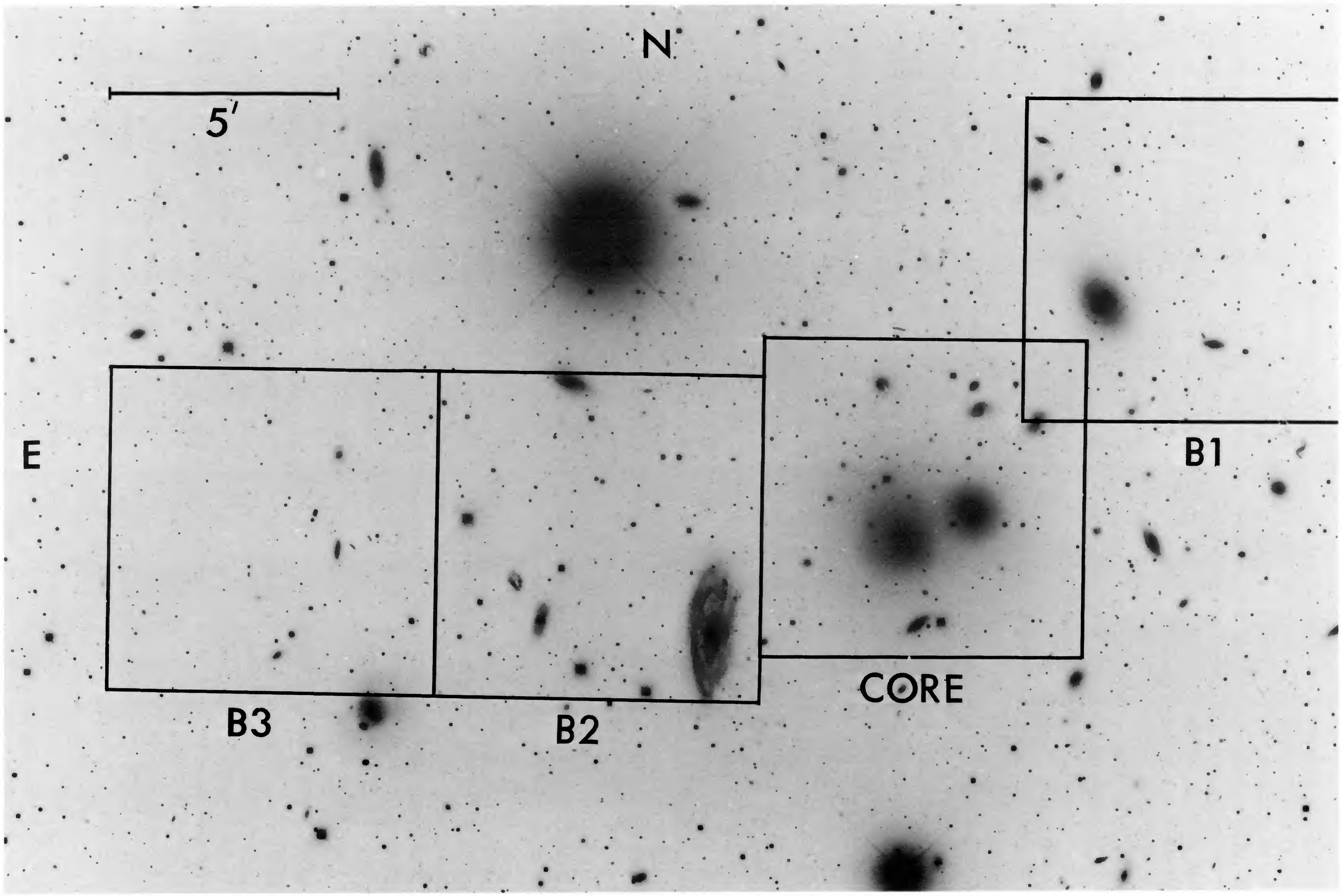

FIG. 1.—Reproduction from CTIO 4 m plate CPF 994 (IIIa-J + GG385), showing the four areas scanned in the present study. Each box is 7.′4 (2000 pixels) square. NGC 3309 and 3311 are in the core region, and NGC 3308 is in region B1.

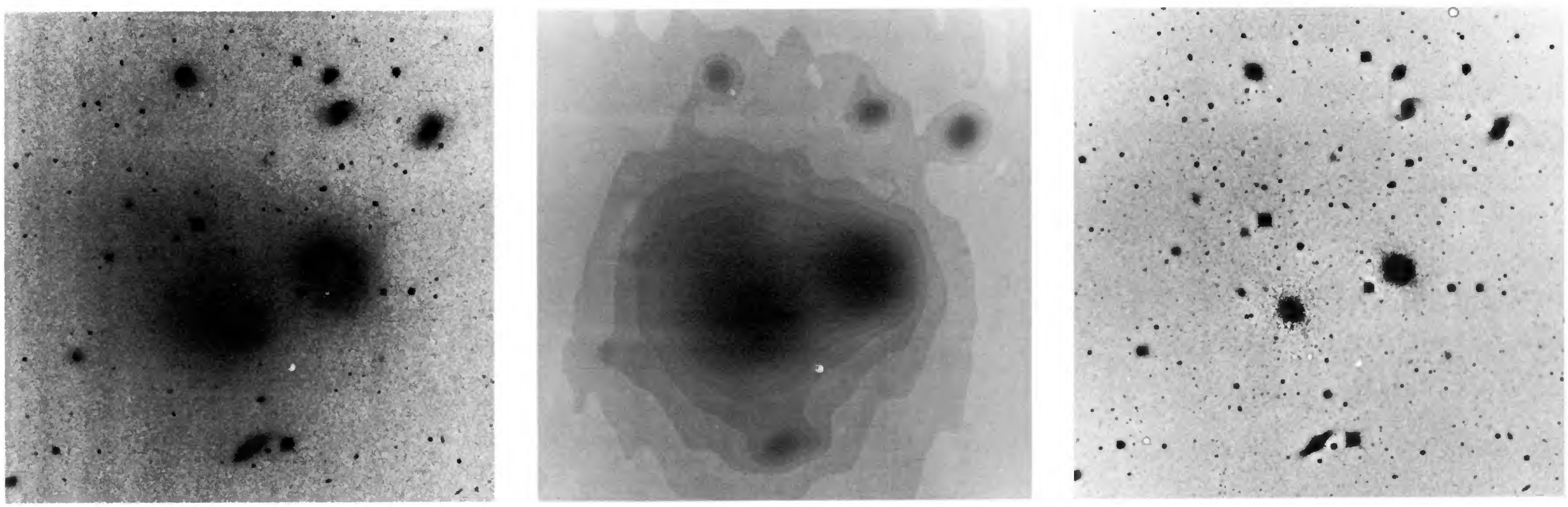

FIG. 2.—Sequence of illustrations of the core field, showing the background flattening and galaxy removal procedure. (*left*) The raw scan frame (in intensity units); (*center*) the "blurred" or isophotal frame generated from the raw scan frame by removal of all small-scale features; and (*right*) the difference between the first two frames, i.e., the "flattened" picture. The last frame is used to carry out the final image detection and photometry.

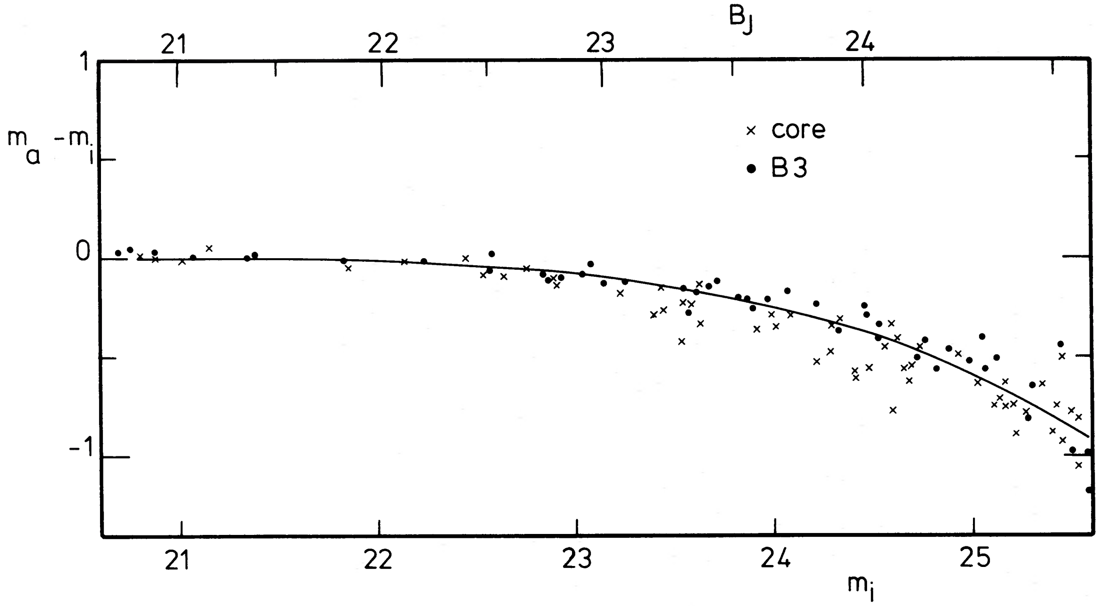

FIG. 3.—Internal calibration of the magnitude measurements. Here m_i is the isophotal magnitude obtained by the sum of all pixel intensities above detection threshold; and m_a is the 2CAP, or concentric aperture, magnitude of the same image. Crosses represent images selected from the core field, and dots, from the B3 field; they refer to a mixture of stellar and (slightly) nonstellar images. The B_J scale at the top indicates how m_i correlates with the final magnitude scale.

PFIND magnitudes (m_i). Since m_i contains only the pixels above a given intensity level, it measures a smaller and smaller fraction of the image for progressively fainter stars and diverges rapidly from a true magnitude scale near the plate limit. Figure 3 displays the difference ($m_a - m_i$) as a function of m_i for a sample of measured images from our studied fields; the expected downturn of m_i toward the plate limit is clearly seen. In addition, m_a and m_i are encouragingly well correlated, with typical scatter of $\sigma \approx 0.10$ mag. We therefore transformed m_i through the mean curve shown in Figure 3 to place it onto the normal m_a magnitude scale.

For absolute calibration of the photometry, we used the Pickering-Racine secondary images of the photoelectric standard stars to make the final transformation of m_a into B_J. The relation $B_J = B - 0.28\ (B - V)$ (cf. Harris and Smith 1981; Stryker 1981; Kron 1980) was used to represent the magnitude system of the (IIIa-J + GG385) combination. The prism constant Δm between primary and secondary images cannot be well determined from the local Hydra sequence (Paper I) because there is little overlap between the primary ($11 < B_J < 18$) and secondary ($B_J > 18$) image sequences; most users of the CTIO prism have measured values in the range $\Delta m = 6.8 \pm 0.1$, which we have adopted here. On plate 994, the secondary images appear structurally indistinguishable from faint primaries, and we have no reason to suspect Δm to be a function of B_J. For the six sequence stars with secondary images in the range $20 < B_J < 23$ (not so close to the plate limit that random errors dominate, but faint enough to be unsaturated), we find the *relative* Δm to be constant within $\sigma(B_J) = 0.035$ mag. In summary, we believe that our adopted magnitude scale is not likely to be incorrect by more than ~ 0.2 mag in either direction; nevertheless, a more securely determined calibration (e.g., by CCD observations) would plainly be desirable in future.

TABLE 1

INTERNAL RANDOM ERRORS OF THE PHOTOMETRY

B_J Magnitude	$\sigma(B_J)$
$\leqslant 22$	0.10
23.0..........	0.20
24.0..........	0.40
24.5..........	0.8:

In Table 1 we summarize our estimates of the photometric errors in the final B_J magnitudes. These were obtained primarily from comparison of a small extra series of measurements on two different plates, combined with the *internal* random errors shown in Figure 3. In this and other related projects, our experience with the IPPS reductions indicates that the aperture-type measurement errors tend to increase very rapidly within ~ 1 mag of the plate limit, essentially because of the difficulty in fixing a valid sky background locally. Errors $\gtrsim 1$ mag can be generated in either direction, depending on whether excessive contamination exists in the star aperture or the sky annulus; these deviations are so large that the quoted individual magnitudes for objects at the plate limit become almost meaningless except for statistical purposes. Image profile fitting would in principle be preferable for the faintest objects (at considerably more expense in computing time). This is simply a restatement of the traditional problem that the limit for useful photographic photometry is significantly brighter than any "detection" limit at which images can just barely be seen to exist. According to our present calibration, images as faint as $B_J \approx 25.0$ were detected in the reduced scans, but we have restricted our discussion to the range $B_J < 24.5$.

III. THE CORE REGION: WHICH GALAXY?

In the core field (see Fig. 1), the two giant elliptical galaxies NGC 3309 and 3311 are separated by only 100″, and it is not immediately obvious to which of the two (if either) the majority of the excess stellar images in the region belong. The two are structurally quite different: NGC 3309 has the appearance of a relatively normal E3 elliptical, whereas NGC 3311 has a much lower central surface brightness and an obvious diffuse envelope reminiscent of a cD-type structure. Their total magnitudes and colors show NGC 3311 to be the most luminous object in the Hydra I system ($B_T = 12.9$, $B - V = 1.03$ for NGC 3309; $B_T = 12.1$, $B - V = 1.03$ for NGC 3311; see Smyth 1983). Van den Bergh (1977*b*) and Smyth (1983) have commented on these characteristics in terms of possibly differing environmental histories. Van den Bergh also notes that, on the basis of rough star counts in the regions close to the centers of each galaxy ($r < 75''$), each of the two appears to have similar numbers of bright clusters. It is also noteworthy here that both NGC 3309 and 3311 have radial velocities within 1 σ of the mean Hydra velocity (V_0 [Hydra] $= 3425$ km s^{-1} and $\sigma = 676$ km s^{-1} for the system as a whole; see Richter, Materne, and Huchtmeier 1982). With $V_0^{3309} = 3801$ km s^{-1} and $V_0^{3311} = 3575$ km s^{-1} (Richter, Materne, and Huchtmeier 1982) NGC 3311 may then be the closer of the two to being at the dynamical center of the system.

Careful inspection of our plate 994 suggests that indeed both galaxies may have clusters associated with them, but that, for the region $\gtrsim 1'$ outside the two galaxy centers, the majority of these images appear to congregate around NGC 3311. A more graphic illustration of this impression is displayed in Figure 4*a*. Here, for the core field containing NGC 3309/3311, we have computer-plotted the positions of all PFIND images detected in the magnitude range $22.0 < B_J < 24.5$. The higher density of images toward the center of the frame is evident, as is their tendency to group around NGC 3311. Circles of radius 150 pixels (34″) around each galaxy center have been excluded, since within these regions the random pixel-to-pixel intensity fluctuation becomes high enough to generate large numbers of false "noise" images. Figure 4*b* provides a similar plot for the background field B3 for comparison.

Our hypothesis is therefore that NGC 3311 dominates the globular cluster population in Hydra. We have checked this claim with the following numerical test of the distribution of images around the field as a function of *position angle*:

1. A 700 pixel radius circle (the largest that can be inscribed within the core field edges) is drawn around each of the two galaxies (3309, 3311), with the region $r < 150$ pixels being excluded as described above.

2. Each circle is divided into 20° sectors, with the position angle $\theta = 0°$ defined as the line between the two galaxy centers (this line runs nearly SE-NW). The angle θ increases counterclockwise, and the two sectors which contain the *other galaxy* (i.e., the other 150 pixel excluded circle) are excluded as well. For the circle centered on NGC 3311, this excluded zone (containing 3309) is $340° < \theta < 20°$, and for the NGC 3309 circle the excluded zone containing NGC 3311 is $160° < \theta < 200°$.

3. The number of detected images (from the PFIND sample) within each sector is then counted and plotted against θ.

The results of this exercise appear in Figure 5 for the two separate circular zones. With our viewpoint centered on NGC 3311 (Fig. 5, *top*), we notice only a uniform distribution of n, with no trends above the sector-to-sector scatter expected from count statistics. The average over all 16 sectors is $\bar{n} = 29.1$, with an rms scatter $\sigma(n) = 5.5$ almost exactly equal to $\bar{n}^{1/2}$. With NGC 3309 as the center (Fig. 5, *bottom*), the result is distinctly different: the highest bins all lie around $\theta = 180°$, and the lowest ones around $\theta = 0°$, with the entire distribution varying roughly sinusoidally with θ. Here, the actual sector-to-sector scatter is $\sigma(n) = 8.0$, roughly twice the statistical deviation $\bar{n}^{1/2} = 4.9$ for a random distribution. The data illustrated in Figure 5 *top* and *bottom* together are just the results expected if the globular cluster images in the field are grouped around NGC 3311 and *not* 3309.

A more specific estimate of the relative numbers of clusters attached to the two galaxies can be made if we fit sine curves to the two $n(\theta)$ graphs. For Figure 5, *top*, we assume a model $n(\theta) = \bar{n} + A \sin\theta$, and for Figure 5, *bottom*, $n(\theta) = \bar{n} - B\cos\theta$. Solving for the amplitudes A and B by least squares gives $A = -0.6 \pm 1.4$, $B = 10.1 \pm 1.1$, and hence $|A/B| = 0.06 \pm 0.14$. This last fraction, which turns out to be almost indistinguishable from zero, gives an approximate idea of the relative numbers of clusters, $N_{\rm cl}(3309)/N_{\rm cl}(3311)$.

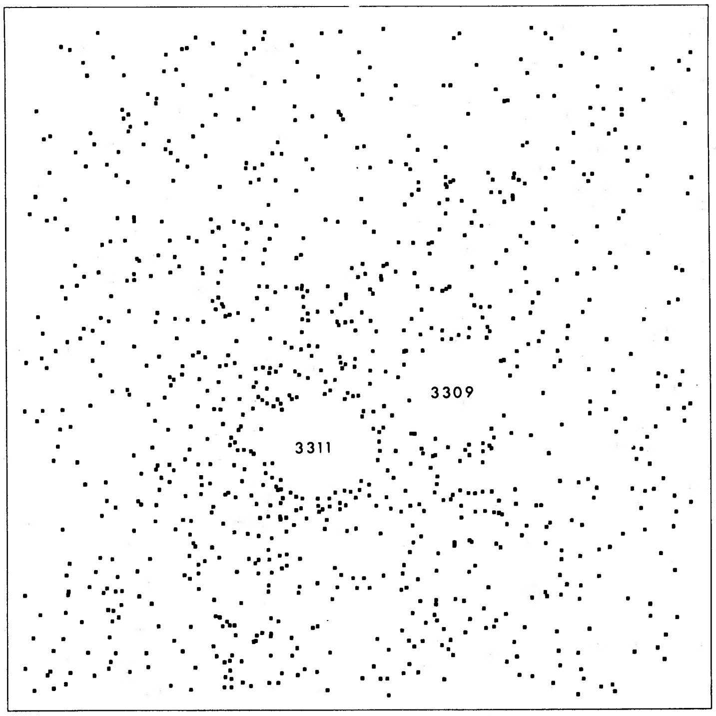

FIG. 4*a*

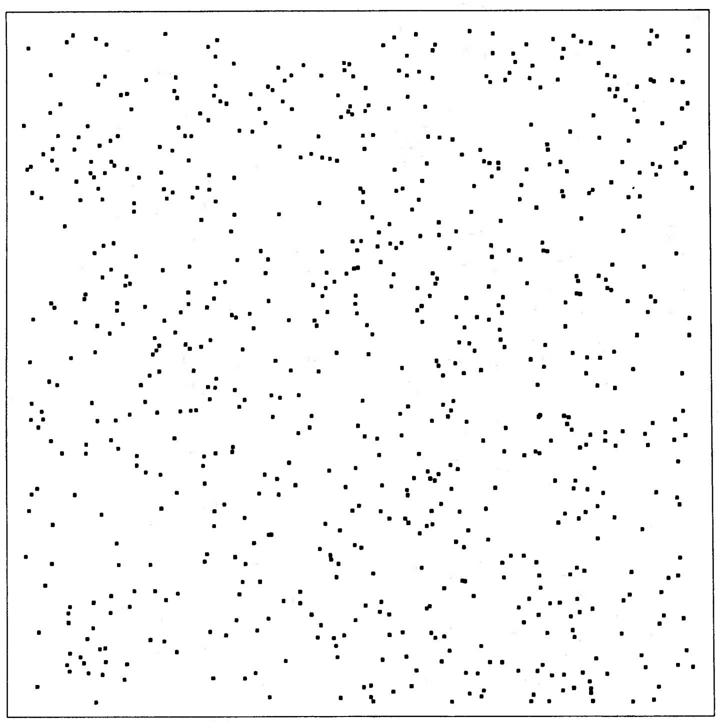

FIG. 4*b*

FIG. 4.—(*a*) Map of images detected by the automated PFIND program in the core field brighter than $B_J = 24.5$. North is at top, and east is at left as in Fig. 1; both stellar and nonstellar images are plotted, without regard to size or magnitude. The excluded circles of radius 150 pixels (0′.56) around both NGC 3309 and 3311 are indicated. Note the preponderance of images concentrated around NGC 3311; see § III of the text. (*b*) Map of all images detected by PFIND in the background field B3, as in Fig. 4*a*.

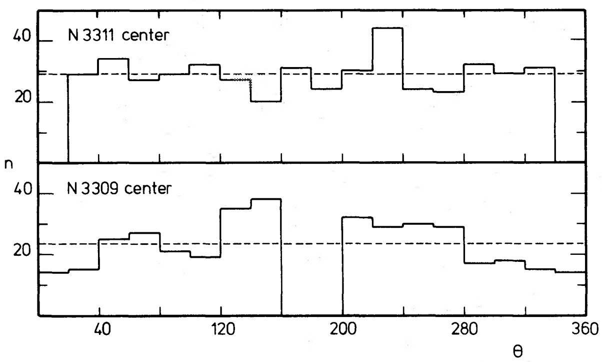

FIG. 5.—Angular distribution of the detected images around NGC 3311 and 3309. Here n is the total number of images in each 20° sector ($150 < r < 700$ pixels) around each galaxy. The top panel shows the results with NGC 3311 at the center of the test circle, and the bottom panel, with NGC 3309 at the center. The line $\theta = 0°$ is defined by the line joining the centers of the two galaxies, with θ increasing counterclockwise. Each panel has two "missing" sectors ($-20° < \theta < 20°$ for the top panel, $160° < \theta < 200°$ for the bottom); these are the sectors containing the other galaxy. The dashed line in each case marks the average $\langle n \rangle$ over all sectors.

The simplest conclusion would then have to be that NGC 3311 contains the majority of the globular clusters in the Hydra system. Of course, one type of distribution that our numerical tests would fail to detect would be a more spread-out population of clusters which is shared equally between these two central galaxies or which belongs to the Hydra Cluster as a whole. There is, however, no evidence for any kind of major interaction between NGC 3309, 3311, or the other large Hydra members (Smyth 1983). The present combination of evidence is more consistent with the picture that NGC 3309 and 3311 are separate systems rather than both being embedded in a larger region of additional material; we then conclude that the globular clusters we now see in the region therefore most likely belong to NGC 3311.

Our adopted result for the present is that NGC 3311 contains $\gtrsim 90\%$ of the globular clusters that are seen in the core Hydra region (excluding the very most central areas around the two giant elliptical galaxies that we have been unable to survey, $r \lesssim 1'$). A final supporting argument for this conclusion will be described in § IV following.

IV. RADIAL DISTRIBUTIONS

a) Observed Distributions and Background

A major goal of our present study was to determine the spatial distribution of the "excess" images (presumed to be globular clusters), to be compared where possible with the distribution of halo light in the parent galaxies. The dominance of NGC 3311 over 3309 in the central Hydra region considerably simplified this problem, and as a first approximation we simply calculated the surface density of all images in the field using NGC 3311 as the center point.

As before, the central circles of radius 150 pixels around both NGC 3311 and 3309 were excluded, and the region around NGC 3311 was divided into concentric annuli. The number density, σ, of images in each radial zone was then plotted as a function of r. The annuli were extended out partially past the borders of the core field, by explicitly calculating the area of intersection of the square frame and the given annulus, where necessary.

Because of practical limitations on computer time and scheduling during our analysis sessions at KPNO, we were able to complete both the PFIND and "manual" 2CAP reductions in strictly comparable ways for just the core and B3 fields (Fig. 1); most of our current results therefore depend on only these two areas. B3 was regarded as the most important of the background areas since it contained no major galaxies and lies $\gtrsim 10'$ (or 100 kpc if Hydra is 35 Mpc distant) away from the core field, distant enough that we expected it to contain a negligible density of Hydra globular clusters itself. The results for the $\sigma(r)$ profile from the PFIND data are summarized in Table 2. Successive columns give the inner and outer radii of the annulus (in pixels), the mean radius of the annulus in arcmin (where $r^2 = [r_{\rm inner}^2 + r_{\rm outer}^2]/2$), the number n of images found in the annulus within the magnitude range $22.0 < B_J < 24.5$, the annular area, and the surface density σ of the counted images. The quoted internal errors on σ simply represent the count statistics, $n^{1/2}$.

Figure 6 shows the $\sigma(r)$ profile through both the core and B3 fields. The prominent rise of σ in toward NGC 3311 confirms the visual impression that this galaxy contains an extensive cluster system. The major puzzle presented by the figure is the identification of some kind of "background" level σ_b which $\sigma(r)$ should ideally approach at large r. From the numbers near the edge of the core field, we would expect to see $\sigma_b \lesssim 9$ arcmin^{-2}, but continuing out through the more distant B3 field we find instead a $\sim 40\%$ higher mean value, $\sigma \approx 13.2$ arcmin^{-2}, with hints of some systematic fluctuations as well.

The discrepancy between the outer core field and B3 might be due to residual photometric differences (for example, B3 could have been sampled to a completeness limit a few tenths of a magnitude fainter), but we believe this possibility to be unlikely. Both areas are well within the normal photometric area of the plate, the sky background surface brightnesses in B3 and around the edges of the core field are too similar to cause any noticeable differences in detection thresholds, and both were measured and reduced identically. Presuming the difference to be real, another and more likely explanation would be that area B3 contains a higher number of small, faint

TABLE 2

RADIAL DISTRIBUTION OF IMAGES AROUND NGC 3311 FROM PFIND

Annulus (pixels)	r (arcmin)	n	Annulus Area[a] ($arcmin^2$)	σ (images $arcmin^{-2}$)
		Core Field		
150–200	0.657	55	0.760	72.37 ± 9.76
200–300	0.948	77	2.171	35.47 ± 4.04
300–400	1.314	76	2.774	27.40 ± 3.14
400–500	1.683	101	3.474	29.07 ± 2.89
500–600	2.053	93	4.438	20.96 ± 2.17
600–700	2.423	100	5.644	17.72 ± 1.77
700–800	2.794	106	6.277	16.89 ± 1.64
800–900	3.165	98	6.188	15.84 ± 1.60
900–1000 ...	3.536	72	5.536	13.01 ± 1.53
1000–1100 ...	3.908	61	5.210	11.71 ± 1.50
1100–1200 ...	4.279	52	4.426	11.75 ± 1.63
1200–1300 ...	4.651	33	3.238	10.19 ± 1.77
1300–1400 ...	5.022	17	1.735	9.80 ± 2.38
1400–1700 ...	5.789	12	1.395	8.60 ± 2.48
		B3 Field		
2800–3000 ...	10.787	18	1.865	9.65 ± 2.27
3000–3200 ...	11.530	74	5.518	13.41 ± 1.56
3200–3400 ...	12.273	85	5.616	15.14 ± 1.64
3400–3600 ...	13.016	79	5.606	14.09 ± 1.59
3600–3800 ...	13.760	86	5.598	15.36 ± 1.66
3800–4000 ...	14.503	83	5.590	14.85 ± 1.63
4000–4200 ...	15.246	61	5.584	10.92 ± 1.40
4200–4400 ...	15.989	74	5.579	13.26 ± 1.54
4400–4600 ...	16.733	60	5.574	10.76 ± 1.39
4600–4800 ...	17.476	71	5.570	12.75 ± 1.51
4800–5000 ...	18.219	39	3.177	12.28 ± 1.97

[a]Some of the annuli cross the excluded 150 pixel circle around NGC 3309 or do not lie completely within the boundaries of the scanned fields. The tabulated areas give the portion of the annulus actually used, corrected for these effects.

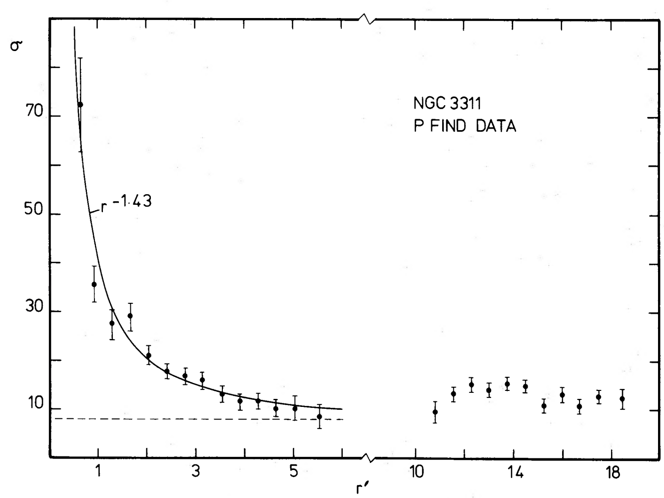

FIG. 6.—Radial distribution of images around NGC 3311, from the PFIND measurements. Here σ is the number of images (of all types) per $arcmin^2$, and r the distance from the center of NGC 3311 in arcmin. Data points for $r < 6'$ are from the core field, and for $r > 10'$ from the B3 field. The adopted background level ($\sigma_b = 8.0$ $arcmin^{-2}$; see text) is shown as a dashed line. The fitted power-law curve is from eq. (2) of the text.

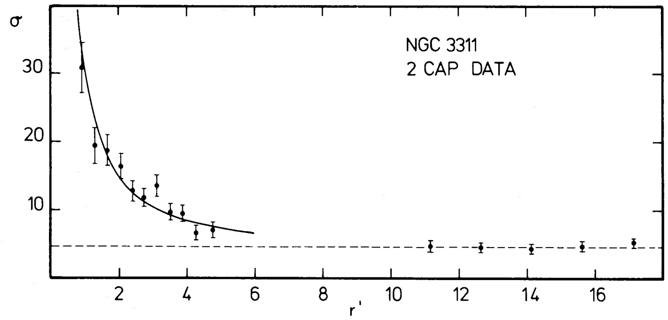

FIG. 7.—Radial distribution of images around NGC 3311, from the manual 2CAP measurements. Notation is as in Fig. 6, except that σ now excludes nonstellar images of size $\gtrsim 2''$. The adopted background level for these data is $\sigma_b = 4.7$ arcmin^{-2}, shown as the dashed line. Note that the innermost annulus of Fig. 6 ($150 < r < 200$ pixels) is not present here; the two data sets do not cover exactly the same radial range.

galaxies (which dominate the image counts for $B_J \gtrsim 23$). Some independent support for this can be found, for example, in the large-area survey of Hewett, MacGillivray, and Dodd (1981), who find that for $B \approx 22$ the number density of galaxy images fluctuates significantly because of clustering and superclustering over scale lengths $\sim 7'$, very near the size of our scan areas. With this picture in mind, it should then be expected *a priori* that our σ_b *should not be well defined* at precisions $\lesssim 20\%$ or so, if the counts include *all* types of images (both stellar and nonstellar). This fundamental problem in determining a valid background afflicts most of the previous star-count studies of globular cluster systems in large galaxies (e.g., Harris and Smith 1976; Harris and van den Bergh 1981), and future work would benefit from more extensive attempts to do star/galaxy image separation (e.g., MacGillivray *et al.* 1976; Jarvis and Tyson 1981).

We were unable to complete an automatic image classification analysis of this type because of both time and software limitations; but our manual 2CAP data, in which the most obvious nonstellar images had been explicitly weeded out, enabled us to make an approximate but still direct test of the situation. Although the magnitude completeness limit (again estimated at $B_J \approx 24.5$) is less well known in the 2CAP sample because of the personal image selection procedure, we need only assume that the 2CAP sample limit is the *same* for both B3 and the core field. The $\sigma(r)$ results for the 2CAP data set are summarized in Table 3 and Figure 7. More than half the images in B3 are easily recognized galaxies, and removing these brings σ_b down to a much more

TABLE 3

RADIAL DISTRIBUTION OF IMAGES AROUND NGC 3311 FROM 2CAP

Annulus (pixels)	r (arcmin)	n	Annulus Area (arcmin^2)	σ (images arcmin^{-2})
		Core Field		
200–300	0.948	67	2.171	30.86 ± 3.77
300–400	1.314	57	2.930	19.45 ± 2.58
400–500	1.683	70	3.720	18.82 ± 2.25
500–600	2.053	75	4.590	16.34 ± 1.89
600–700	2.423	72	5.644	12.76 ± 1.50
700–800	2.794	74	6.277	11.79 ± 1.37
800–900	3.165	84	6.188	13.58 ± 1.48
900–1000 ...	3.536	53	5.536	9.57 ± 1.32
1000–1100 ...	3.908	49	5.210	9.41 ± 1.34
1100–1200 ...	4.279	29	4.426	6.55 ± 1.22
1200–1400 ...	4.780	35	4.973	7.04 ± 1.19
		B3 Field		
2800–3200 ...	11.18	35	7.38	4.74 ± 0.80
3200–3600 ...	12.66	52	11.22	4.63 ± 0.64
3600–4000 ...	14.15	48	11.19	4.29 ± 0.62
4000–4400 ...	15.63	52	11.16	4.66 ± 0.65
4400–4800 ...	17.12	58	11.14	5.21 ± 0.68

uniform and well-defined level in comparison with Figure 6. Just as important is that the *same* curve (see below) describing $\sigma(r)$ for the NGC 3311 globular clusters in the core field can be applied successfully to both Figures 6 and 7. In summary, our available evidence strongly indicates that the faint-galaxy images contribute most of the "noise" in the $\sigma(r)$ determination, and that the space distribution of the NGC 3311 cluster system obeys a smooth falloff with r out to large distances.

b) *Radial Profiles*

We may now attempt to derive the actual density profile of the cluster system, $\sigma_{cl}(r) = \sigma(r) - \sigma_b$, more specifically. To model the shape of $\sigma_{cl}(r)$, previous studies (e.g., Harris and Smith 1976; de Vaucouleurs and Buta 1978; HR; Harris and van den Bergh 1981) indicate that we might choose either a simple power law ($\sigma_{cl} \sim r^{-\alpha}$) or a de Vaucouleurs $r^{1/4}$ law ($\log \sigma_{cl} = a + br^{1/4}$). In fact (as will be seen), the observational errors in the Hydra data do not allow a clear preference for either formulation; the main advantage of the power-law form is that it allows structural features of the system, such as the central concentration, to be more easily specified and compared.

The 2CAP data are straightforward to handle. From Table 3 and Figure 7, we adopt $\sigma_b(\text{2CAP}) = 4.7 \pm 0.3$ (the average of the bins in B3) and subtract this from the $\sigma(r)$-values in the core field to yield the run of $\sigma_{cl}(r)$. Least squares solutions for each of the two models then give

$$\log \sigma_{cl} = (1.45 \pm 0.09) - (1.44 \pm 0.19) \log r \quad \text{(power law)}, \quad (1a)$$

or

$$\log \sigma_{cl} = (3.50 \pm 0.25) - (2.07 \pm 0.28) r^{1/4} \quad \text{(de Vaucouleurs law)}. \quad (1b)$$

These solutions appear graphically in Figure 8. It can be seen that either formulation adequately represents the data.

The PFIND data (Table 2 and Fig. 6) present a more difficult situation since the cluster system plainly extends beyond the boundaries of the core field, and B3 is not useful for defining the appropriate σ_b. Nevertheless, from the core field alone a *self-consistent* result for $\sigma_{cl}(r)$ can still be obtained in the following manner:

1. An initial guess at σ_b is made [e.g., from the value of $\sigma(r)$ near the edge of the field], and this quantity is then subtracted from $\sigma(r)$ everywhere to give a first estimate of $\sigma_{cl}(r)$.

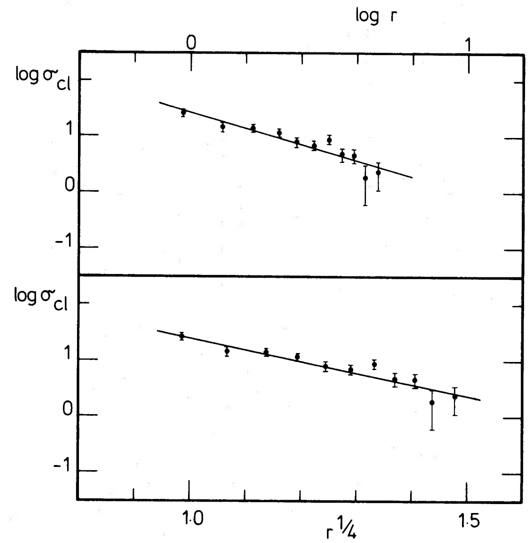

FIG. 8.—Radial profile of the NGC 3311 globular cluster system, from the 2CAP data. Here $\sigma_{cl} = \sigma - \sigma_b$ is in objects per arcmin^2. The upper panel shows $\log \sigma_{cl}$ vs. $\log r$ (power law), and the lower panel shows $\log \sigma_{cl}$ vs. $r^{1/4}$ (de Vaucouleurs law), in both cases for r in arcmin. The least squares solutions of eq. (1) are shown as the fitted lines.

2. Assume *either* that $\sigma_{cl}(r)$ matches a power law *or* an $r^{1/4}$ model over its entire range. Since the inner points which lie well above background are little affected by the choice of σ_b, they can be used to estimate the correct slope of the ($\log \sigma$) graph.

3. The adopted value of σ_b can then be revised, and the solution iterated until $\log c_{cl}$ obeys a single straight-line falloff over all r. The solution for the appropriate σ_b and $\sigma_{cl}(r)$ of course converges rapidly after one or two starting guesses.

With these assumptions, the PFIND data in the core field yield $\sigma_b = 8.0 \pm 2.0$ arcmin^{-2} (for *either* the power law or $r^{1/4}$ model) and the following solutions f or σ_{cl}:

$$\log \sigma_{cl} = (1.52 \pm 0.04) - (1.43 \pm 0.10) \log r \quad \text{(power law)}, \quad (2a)$$

or

$$\log \sigma_{cl} = (3.68 \pm 0.17) - (2.15 \pm 0.14) r^{1/4} \quad \text{(de Vaucouleurs law)}. \quad (2b)$$

Within the errors, these curves (graphed in Fig. 9) are entirely consistent with the 2CAP results in equation (1). The $\sigma_{cl} \sim r^{-1.43}$ curve is drawn as well in both Figures 6 and 7 over the core-field data points.

A quick but important additional check that the 2CAP and PFIND data samples in fact have the same effective "plate limits" can be made in the following way. We calculate the ratio $a_{cl} \equiv \sigma_{cl}(\text{PFIND})/\sigma_{cl}(\text{2CAP})$

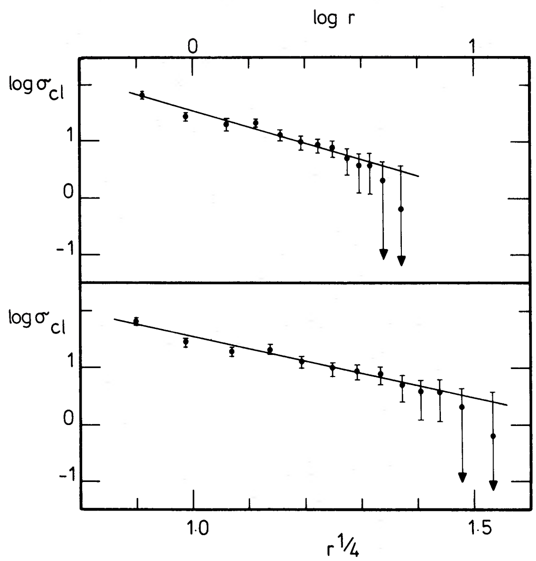

FIG. 9.—Radial profile of the NGC 3311 globular cluster system, from the PFIND data. Notation is as described in Fig. 8; the fitted lines are those of eq. (2).

from Tables 2 and 3, with the σ_b values as used above. Calculating this ratio for each annulus from 200 to 1200 pixels and weighting each annulus inversely as $\varepsilon(a_{\rm cl})^2$, we find the mean over the whole core field is $\overline{a_{\rm cl}} = 1.13 \pm 0.12$. (Since most of the weight in this average comes from the inner rings, this result is not particularly sensitive to the adopted σ_b's.) Then, noting that the relative numbers of clusters increase with magnitude roughly as $(\Delta \log N)/\Delta B_J \approx 0.6$ (see § V and Table 4), we estimate that the PFIND sample reaches deeper than the 2CAP sample by $\sim (0.1 \pm 0.1)$ mag. The effective limits of the two samples are therefore satisfactorily close.

Since $\sigma_b(\text{2CAP}) \sim 5$ arcmin^{-2} and $\sigma_b(\text{PFIND}) \sim 8$ arcmin^{-2} at comparable plate limits, we would deduce that 2CAP has removed ~ three galaxy images per arcmin^2 *in the core field*. By comparison, Jarvis and Tyson (1981), with an automated star/galaxy image classification algorithm, have found approximately five to six galaxies per arcmin^2 over the same magnitude interval ($22.0 < B_J < 24.5$, making a reasonable extrapolation of their data past $B_J = 24.0$) from several high-latitude fields. Even after accounting for the lower galactic latitude of the Hydra field, it seems clear that the 2CAP sample still contains ~ two to three nonstellar images per arcmin^2, and that a rigorous image classification technique would substantially refine the results.

TABLE 4

LUMINOSITY DISTRIBUTION OF THE GLOBULAR CLUSTERS

B_J Interval	$\phi_{\rm cl}$(arcmin^{-2})
22.00–22.49 ...	0.28 ± 0.23
22.50–22.99 ...	0.76 ± 0.34
23.00–23.49 ...	1.04 ± 0.43
23.50–23.99 ...	2.38 ± 0.56
24.00–24.49 ...	5.63 ± 0.80

c) The NGC 3309 Problem

The potential contamination introduced by the neighboring elliptical galaxy NGC 3309 remains a nagging doubt in the radial profile analysis. In § III we attempted to show that NGC 3311 dominates the globular cluster population in the region, so that any contributions from globular clusters belonging to NGC 3309 should not change the above results for $\sigma_{\rm cl}$ (3311) by more than ~ 10% at any r. However, one additional way of demonstrating this is to re-derive $\sigma_{\rm cl}(r)$ for NGC 3311 by using only the *east* part of the core field. That is, we draw a north-south line through the NGC 3311 center and calculate the density distribution of points to the left of that line in Figure 4. In this region, any contamination from NGC 3309 will be greatly reduced.

The results of this exercise are shown in Figure 10, which should be compared directly with Figure 6. Exactly the same power-law curve from equation (2a) is drawn over the data points in both graphs (where $\sigma_b = 8.0$ arcmin^{-2} for both). Aside from the larger error bars in Figure 10 because of the smaller number of images in

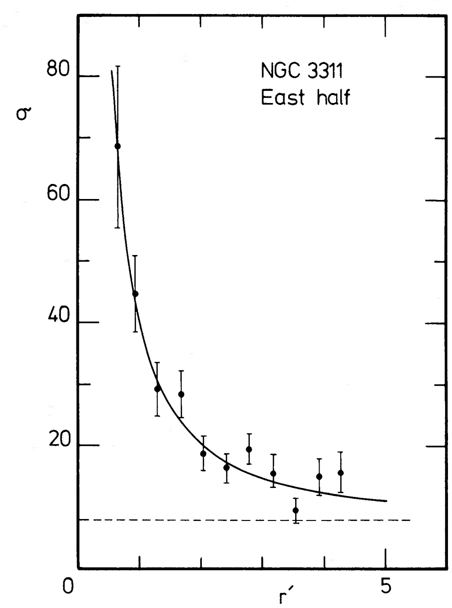

FIG. 10.—Radial distribution of PFIND images around NGC 3311, using only the part of the core field east of the NGC 3311 center. Compare with Fig. 6; the same background level and fitted power-law curve are drawn in. This graph indicates that any clusters from NGC 3309 are not introducing serious contamination; see § IV*c*.

the sample, there is little to choose between the two representations. To the best of our present knowledge, therefore, we believe that NGC 3309 does not exert important effects on our radial profile analysis of NGC 3311.

An unfortunate consequence of this result is that we are unable to make any statements about the globular cluster system (if any) around NGC 3309. Aside from counts of objects in the very central regions of the galaxy (which might be obtained by future CCD observations, for example), the NGC 3311 cluster system dominates the region so completely that any such data on NGC 3309 will be difficult indeed to obtain.

d) *Comparison with Halo Light*

In several previous studies (e.g., Harris and Smith 1976; Hanes 1977; Harris and Petrie 1978; HR; Forte, Strom, and Strom 1981), deliberate attempts have been made to compare the total extent and central concentration of globular cluster systems in Virgo and other elliptical galaxies with the halo light of the parent galaxy. Any structural differences which appear between these two types of Population II objects may be interpreted as evolutionary distinctions, e.g., that the clusters and the halo *stars* were formed at separate epochs (HR; Strom *et al.* 1981).

The available surface photometry of NGC 3311 is summarized and thoroughly discussed by Smyth (1983), who has used photoelectrically calibrated measurements from photographic plates to derive the halo light profile. In Figure 11 we compare Smyth's B halo profile for NGC 3311 with our $\sigma_{\rm cl}(r)$ (from Fig. 9), where the intensity curve $\mu_B(r)$ has been arbitrarily normalized along the vertical axis to match the cluster data. The two radial distributions fit satisfactorily within their own internal errors, and to a first approximation we conclude that both these types of Population II objects follow the same spatial distribution. However, for $\log r \gtrsim 0.4$ the observational uncertainties in both the cluster counts and the halo light intensity become large enough to mask any differences between them at the level of $\Delta\alpha \sim \pm 0.3$ or so in the power-law slope. In future work with a more refined understanding of the background, for example, it would be of great interest to see whether the cluster distribution may actually be slightly flatter than the halo light, as seems to be the case for M87 (HR; Strom *et al.* 1981), or whether the clusters might even follow the mildly triangular-shaped isophotal structure around $r \sim 3'$ that is noted by Smyth (1983).

e) *NGC 3308*

The third largest central Hydra I elliptical galaxy is NGC 3308, to the northwest in our field B1 (Fig. 1). Our reduction of the plate scan in B1 was not strictly comparable to either the core or B3 field (the details of the sky-flattening procedure were different, and the area was not surveyed to the same measured magnitude limit). Nevertheless, we were able to plot the number of detected images around NGC 3308 in the radial range $150 < r < 1600$ pixels within B1, to test for the presence of globular clusters. The resulting $\sigma(r)$ curve (from the PFIND measurements, down to a completeness limit $B_J \lesssim 24.0$) shows no systematic inward increase. The innermost point, for the 150–200 pixel annulus, is based on only 10 counted objects and is clearly not statistically significant. The average of the other bins is $\langle\sigma\rangle = (5.43 \pm 0.33)$ arcmin^{-2}, as shown by the line in Figure 12.

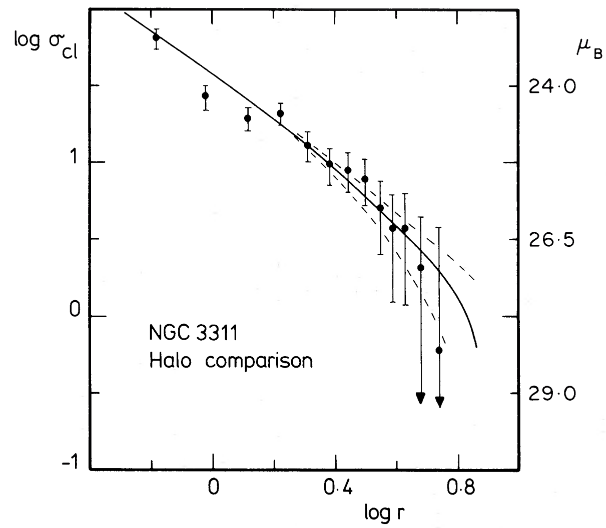

FIG. 11.—Comparison of the cluster distribution around NGC 3311 with its halo light intensity μ_B (Smyth 1983). The μ_B curve (*solid line*) has been normalized arbitrarily by setting $\log \sigma_{\rm cl} = 1.5$ equivalent to $\mu_B = 24$ mag arcsec^{-2}. Dashed lines indicate Smyth's estimated internal errors in the surface photometry.

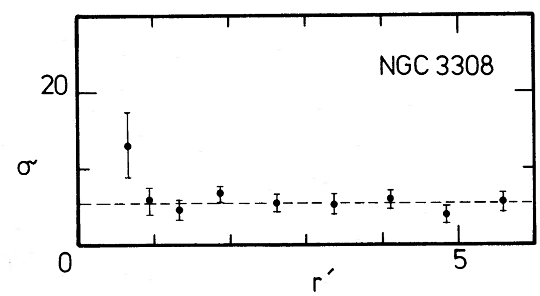

FIG. 12.—Radial distribution of images around NGC 3308 (field B1), down to $B_J(\lim) = 24.0$. The background level $\sigma_b = 5.5$ arcmin^{-2} is shown; see § IV*e*. No significant cluster system is evident.

V. THE CLUSTER LUMINOSITY DISTRIBUTION

In this section, we investigate the magnitude distribution of the NGC 3311 globular clusters. The basic interest in this quantity is its potential use as a standard candle for independent distance determination (Hanes 1979; HR), as well as a test of the belief that the clusters behave similarly in all (or most) galaxies. With our considerably larger amount of data compared with Paper I, we attempt a more complete discussion of these points; but as will be seen below, the results are still too uncertain to permit more than rough limits to be set on the Hydra distance.

For the PFIND data, we again encounter the problem that the comparison field B3 does not adequately represent the background number density of images in the *local* region around NGC 3311, where most of the clusters are. Thus we cannot simply subtract the average σ(B3) from σ(core) at each magnitude level B_J. On the other hand, the 2CAP data do not have as well defined a magnitude completeness or cutoff limit, and it is critically important to establish the run of $\sigma_{cl}(B_J)$ as faint as possible since Hydra is so distant. We have therefore taken the PFIND data set and used the outer parts of the core field itself to estimate the *local* background luminosity function, $\sigma_b(B_J)$ (see Hanes 1977 and Strom *et al.* 1981 for a similar approach with respect to M87 and the other Virgo ellipticals). Within the core field, we define two concentric annuli about NGC 3311 ($r_1 < r \leqslant r_2$ inner, and $r_2 < r \leqslant r_3$ outer) and calculate the average number density of images within each of the two annuli, $\sigma_{12}(B_J)$ and $\sigma_{23}(B_J)$, as a function of magnitude. The *difference* between these, $\phi_{cl}(B_J) = \sigma_{12}(B_J) - \sigma_{23}(B_J)$, should then cancel out the background σ_b and give an unbiased estimate of the cluster luminosity function to within a constant scale factor. This will be true as long as (a) the background (due mostly to nonstellar images) does not fluctuate significantly between the annuli, and (b) there is no strong variation of $\sigma_{cl}(B_J)$ with *radius* from NGC 3311. Problem (b) is a question we cannot address here, although no such galactocentric variation has been seen in our own Galaxy (HR) or M87 (Strom *et al.* 1981).

Our results for this exercise are summarized in Table 4 and Figure 13. The boundaries of the annuli were set at $r_1 = 150$ pixels, $r_2 = 800$ pixels, $r_3 = 1400$ pixels to make the annular areas approximately equal. In Figure 13, the error bars contain the combined errors in both σ_{12} and σ_{23}. Rather than the abrupt jump in numbers near $B_J \approx 24$ noted in Paper I—which was probably a simple consequence of the small sample for both the clusters and the adopted background—we see here a steady increase in ϕ_{cl} from $B_J \approx 22.5$ to the limit of measurement.

To use the NGC 3311 $\phi(B_J)$ distribution as a distance estimator, we have matched it to the $\phi(B_J)$ curve for the combined globular cluster populations in the brightest Virgo elliptical galaxies (HR; Hanes 1979). This procedure then gives just the *relative* distance modulus between Hydra and Virgo, but its principal advantage is that the same types of parent galaxies (giant ellipticals) are being strictly intercompared without introducing other types from the Local Group. (We note that the shape of the "standard" Virgo/Local Group cluster distribution can be successfully described by a simple Gaussian curve with mean $\overline{M}_J \approx -6.8$ and dispersion $\sigma \approx 1.2$ mag [HR; Hanes 1979, 1982], but our discussion here does not rely on this particular model in any way since we employ only the directly *observed* Virgo curve. It will be obvious from Figure 13 that a wide variety of shapes—power laws, Gaussians, etc.—might easily be fitted through the NGC 3311 data points because of their relatively large internal errors and short magnitude range. That is, the Hydra data alone give almost no information on the *intrinsic* shape of the distribution function near its bright end.) To perform the fit, we take $\phi(B_J)$ (Virgo) and shift it fainter by various amounts to obtain the best match to the Hydra data. In the ($\log \phi$, B_J)-plane a corresponding vertical shift is also necessary, but this indicates just the relative total numbers of clusters in each sample.

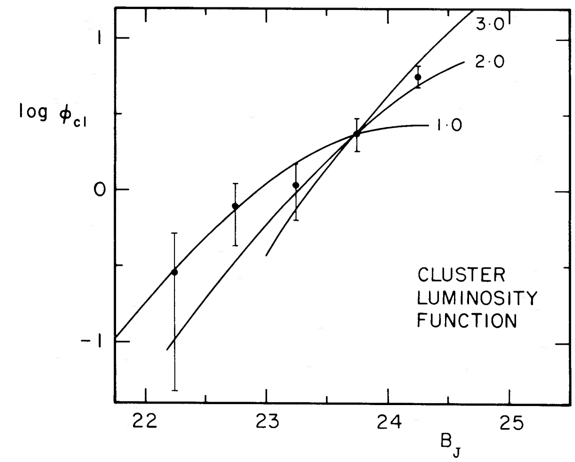

FIG. 13.—Luminosity function for the NGC 3311 globular clusters. Here ϕ_{cl} is the number of clusters per arcmin^2 in each half-magnitude interval, from Table 4. The fitted lines represent the standard Virgo/Local Group luminosity function for globular clusters for three different adopted distances: $\Delta(m - M)$(Hydra-Virgo) = 1.0, 2.0, and 3.0 mag.

The lines in Figure 13 show our "best" distance fits, for adopted distance modulus shifts of $\Delta(m - M)$ (Hydra-Virgo) = 1.0, 2.0, and 3.0 mag. These curves illustrate the representative range of possibilities that we believe are reasonably allowed by the observations. As noted above, the range is so large because we are seeing only the top ~ 2 mag of the cluster luminosity function (with substantial internal errors), so that the fitting procedure cannot make full use of the entire $\phi(M)$ curve shape. Only the change in slope of ($\log \phi$) as it approaches its peak or "turnover" enables rough constraints on the Hydra distance to be made. If $(m - M)_J$(Hydra) ≈ 32.7 (see below), then the peak of the distribution will be expected to appear at $B_J \approx 26.0$, well below our detection limit. At that distance, the brightest observed clusters in NGC 3311, at $B_J \sim 22.5$, would have absolute magnitudes $M_{B_J} < -10$, consistent with the most luminous known globular clusters in our Galaxy and M31.

For $\Delta(m-M)_J = 2.0 \pm 1.0$, then d(Hydra)/d(Virgo) ≈ 2.3 ($+1.3$, -0.8), assuming E_{B-V}(Hydra) = 0.07 and E_{B-V}(Virgo) = 0.02 from their galactic latitudes of 27° and 75° (e.g., Sandage and Visvanathan 1978). If we adopt d(Virgo) ≈ 15 Mpc following Aaronson *et al.* (1980, 1982) and Mould, Aaronson, and Huchra (1980), then d(Hydra) ≈ (35 ± 15) Mpc. In turn, the uncorrected Hubble ratio for Hydra would be $H_0 = V_0/d \approx (100 \pm 40)$ km s^{-1} Mpc^{-1}, with $V_0 = (3425 \pm 34)$ km s^{-1} (Richter, Materne, and Huchtmeier 1982). If instead d(Virgo) ≈ 20 Mpc following Sandage and Tammann (1974), then d(Hydra) ≈ (47 ± 20) Mpc and H_0(Hydra) ≈ 73 ± 30. Correcting V_0(Hydra) for any systematic motion of the Local Group, which might be in the range ~ 200–600 km s^{-1}, measured as either a Virgocentric "infall" motion (Aaronson *et al.* 1980, 1982) or motion with respect to the cosmic background radiation (Boughn, Cheng, and Wilkinson 1981), would serve to raise these estimates of H_0 by $\lesssim 10\%$. In any case, our derived ratio d(Hydra)/d(Virgo) ≈ 2.3 is substantially smaller than the observed *velocity* ratio v_r(Hydra) /v_r(Virgo) = 3.2 ± 0.1, and so adds some support (albeit weak, because of the large uncertainty in d) for the current view of the local Hubble flow as anisotropic (cf. the references above).

Our quoted results formally favor a "high" Hubble constant $H_0 \sim 100$, but it should already be clear from the preceding analysis that values as low as $H_0 \approx 50$–70 (i.e. Hydra distances of 50–70 Mpc) *cannot be ruled out* with any certainty. Major steps toward improving the result could be taken by obtaining photometry around NGC 3311 to the same limit as we have now but with a firmer calibration, over a wider field, and with unbiased stellar/nonstellar image separation. With such material we believe it should become possible to reduce the $\Delta(m-M)$ fitting error in Figure 13 to something approaching ±0.5 mag and hence to obtain a considerably sharper distance estimate. Eventual fainter observations from space reaching the turnover region of the $\phi(B)$ curve would improve the situation still further.

VI. TOTAL POPULATIONS AND SPECIFIC FREQUENCIES

Our final point of concern in this study is the total size of the cluster population of NGC 3311 and comparison with other systems. A useful quantity here is the number of globular clusters per unit galaxy luminosity or "specific frequency" S, which has been defined to intercompare cluster systems in elliptical galaxies of different luminosities (Harris and van den Bergh 1981; Harris 1981). As shown in the earlier studies cited, for the great majority of "normal" elliptical galaxies in Virgo and elsewhere the typical specific frequency is $S_{av} \approx 5$ (normalized to M_v[galaxy] = −15). For M87, the most outstanding anomalous case known, S is ~ 20.

To estimate S for NGC 3311 we need to correct approximately both for the cluster population below the completeness limit of our study and for the radial regions around NGC 3311 ($r < 0'.6$, $r > 5'.0$) that were *not* measured. The first correction is made by assuming a distance to the galaxy and then applying the standard luminosity function for globular cluster systems to estimate the total population over all magnitudes (see HR or Harris and van den Bergh 1981). The area correction can be crudely estimated by extrapolating the observed $\sigma_{cl} \sim r^{-1.4}$ curve (see § IV) both inward and outward from our survey boundaries and adopting some arbitrary radial cutoffs. This approach is likely to be dangerous if relied on in any detail, since we do not know the actual form of $\sigma_{cl}(r)$ at very large or small r. Integrating equation (1a) over $0'.2 < r < 10'$ (or ~ 2–100 kpc if $d \sim 35$ Mpc), we find that the *observed* radial range in our core field (~ 0'.5–5'.0, or 150–1500 pixels) represents only ~ 30% of the total cluster population if the same $\sigma(r)$ curve is valid throughout. A very rough check on this adjustment factor can be made by analogy with our own Galaxy: within 5–50 kpc of the galactic center (which again corresponds to our observed radial region around NGC 3311 for $d = 35$ Mpc), we find ~ 45% of all the globular clusters in the halo (Harris 1976). For the present, we shall estimate the population totals *without* a specific area correction, but with the knowledge that such totals are likely to be incomplete by a factor of ~ 2 or more.

Although our measurements extend to $B_J = 24.5$, we more conservatively set our "completeness" limit for this purpose at $B_J = 24.0$ in view of the photometric errors and image detection/measurement problems that increase so rapidly fainter than this. Then from Tables 2 and 4, within $22 < B_J < 24$ and $0'.5 < r < 5'.0$ we find a total $N = 290 \pm 42$ excess observed images with the adopted background described in § IV. [This total is calculated by multiplying $\sigma_{cl}(r)$ in each annulus by the *total* geometric area of the annulus and not just the portion of this area that lay within the core field boundary. Thus N is larger than the actual number of excess images within the core field itself.] The last half-magnitude interval, 24.0–24.5, would contribute $\gtrsim 350$ more images, or an additional 120% to the total.

The specific frequency is defined as $S = N_{cl} \times 10^{0.4(M_V^T + 15)}$, where N_{cl} is N corrected over all magnitudes at the adopted distance. The final ingredient required is the total galaxy luminosity M_V^T, taken as the light within the standard isophote $D(0)_{25}$. Following Smyth (1983), for NGC 3311 we take $B_T = 12.1$, ($B-$

$V)_T = 1.03$, and hence $V_T \approx 11.1$. For our fiducial distance $d = 35$ Mpc and $A_V \approx 0.2$ mag, this corresponds to $M_V^T \approx -21.8$, a luminosity which is quite comparable to the large elliptical galaxies in Virgo but not exceptionally bright for cD-type objects (see Smyth 1983).

Table 5 summarizes the calculated S-values for four different assumed Hydra distances. Each tabulated S' (where the primed symbol denotes S *without* area correction) has an *internal* uncertainty of approximately $\pm 30\%$ simply because of the internal errors in $V_T(\pm 0.3$ mag) and $N(\pm 15\%)$. However, these uncertainties act only to slide the entire scale of S-values up or down; Table 5 shows mainly how S' changes with the assumed distance d. Because we are sampling only the bright end of the cluster distribution, the luminosity-function correction changes faster with d than does the galaxy luminosity M_V^T, and so in this case S' ends up being a more sensitive function of distance than in closer galaxies (cf. Harris and van den Bergh 1981). However, the results are *not* significantly affected by our exclusion of the last magnitude bin, $24.0 < B_J < 24.5$: putting this back in to the totals does not alter any of the final S'-values in Table 5 by more than 20%. Finally, it is important to repeat that any area correction (which we estimate to be $\gtrsim 2$) would raise S proportionately from the numbers in Table 5.

For *any* reasonable choice of distance, Table 5 indicates unambiguously that S(NGC 3311) is far above the range ($S \sim 5$) occupied by the majority of elliptical galaxies and falls in the region ($S \gtrsim 20$) previously occupied only by M87. We believe that this is one of the clearest results of our present study.

A quick confirmation of the essential point that S(M87) and S(NGC 3311) are similar can be made by a much shorter argument. If $\Delta(m - M)_J$(Hydra-Virgo) = 2.0, then our sample limit of $B_J = 24.5$ corresponds to $B_J = 22.5$ for M87. To this limit, Hanes's (1977) data suggest that there should be ~ 400 clusters within $r \approx 7'.0$ of M87. By comparison, from our Table 2, we find that within $7'.0/2.3 = 3'.0 \approx 800$ pixels of NGC 3311, there are (400 ± 60) clusters above background, which is similar to the M87 total within the combined errors. Since NGC 3311, at $M_V^T \sim -22$, appears to be intrinsically somewhat less luminous than M87 (at $M_V^T \sim -22.3$), then we would conclude NGC 3311 is at least as rich as M87 in globular clusters *per* unit halo luminosity.

TABLE 5

SPECIFIC FREQUENCY OF THE GLOBULAR CLUSTER POPULATION

Assumed Distance	M_V^T	N_{cl}[a]	S'[a]
25 Mpc......	−21.1	2800 ± 400	10
35 Mpc......	−21.8	8000 ± 1200	15
45 Mpc......	−22.4	29000 ± 4200	32
55 Mpc......	−23.0	76000 ± 11000	48

[a] S' does not include area correction factor; see text.

In § III, we concluded that NGC 3309 contained less than 20% (to a $\sim 2\,\sigma$ level) of the globular clusters in the core field. According to Smyth (1983), it is also 0.6 mag (or ~ 1.7 times) fainter than NGC 3311. Combining these numbers with the results of Table 5 then suggests that we can estimate an *upper* limit of S'(NGC 3309) $\lesssim 5$ (again uncorrected for area) for $d = 35$ Mpc. This limit would be entirely consistent with NGC 3309 containing a more-or-less "normal" population of globular clusters, resembling the majority of the Virgo elliptical galaxies, and that it has simply been overwhelmed from our viewpoint by being adjacent to the "supergiant" cluster system of NGC 3311.

In summary, NGC 3311 and M87 appear to exhibit some striking parallels but also certain puzzling differences. Their positions and radial velocities are near the dynamical centers of the clusters, and each have extended halos indicative of the cD phenomenon (Smyth 1983; Oemler 1976). Both contain the only known true "supergiant" globular cluster systems. But Smyth (1983) has emphasized that NGC 3311 is structurally quite unlike M87 or other more normal large ellipticals, having a far lower than normal surface brightness and a generally more diffuse central structure than other D or cD galaxies. Van den Bergh (1977*a*), Smyth (1983), and Forte, Martinez, and Muzzio (1982) discuss the implications of these characteristics for the general model that giant galaxies in the centers of large clusters can grow by accretion and/or infall of surrounding material. In any event, it does not seem plausible that M87 and NGC 3311 can have shared the same histories in any detail given their large structural differences. For this reason, it may be necessary to postulate that the anomalously large globular cluster systems that they both contain arose during their earliest epochs of star formation, and not as a result of special subsequent histories in their surrounding environments.

VII. SUMMARY

Our photometric survey down to $B_J(\text{lim}) \approx 24.5$ in the central region in the Hydra I cluster of galaxies indicates that the brightest galaxy in the system, the cD-like NGC 3311, contains an extremely populous halo of globular clusters. Its brightest clusters appear in significant numbers for $B_J > 22$, increasing steadily to the magnitude limit of our study. We have not been able to detect significant numbers of globular clusters around the other two large elliptical galaxies in the Hydra core, NGC 3308 and 3309. The spatial distribution of the images in our studied area also suggests that the NGC 3311 cluster system follows a radial distribution $\sigma \sim r^{-1.4}$ similar to the halo light of the galaxy itself.

Our comparison of the magnitude distribution of the NGC 3311 clusters with the Virgo globular cluster luminosity function has been used to make a rough distance estimate to Hydra. With the assumptions that the two distributions are intrinsically similar, and that d(Virgo) $\approx$ 15 Mpc, the "best fit" distance to NGC 3311 is $d \approx 35$ Mpc. This result lends additional (though weak) support to the general picture that the Local Group must have a significant local (Virgocentric) motion relative to the overall Hubble flow. For Hydra I, at a redshift $V_0 \approx 3400$ km s^{-1}, our distance measurement under the foregoing assumptions yields an (uncorrected) Hubble ratio $H_0 \approx 100 \pm 40$.

Finally, regardless of the details of the distance estimate, we find that the total number of globular clusters in NGC 3311 is fully comparable to that in only one other galaxy, M87 (specific frequency $S \sim 20$, or perhaps higher if full area corrections are made). The well-known M87 anomaly of a "supergiant" globular cluster system is therefore no longer a unique phenomenon. However, M87 and NGC 3311 are structurally so dissimilar (despite both being dominant elliptical galaxies near the center of a large cluster) that their especially large globular cluster populations may most likely have arisen near their initial star-forming epoch rather than acquired later by environmental processes.

Insofar as is possible at present, we have attempted to interpret the results in ways that do not depend strongly on the details of our magnitude calibration and plate measurement procedure. Nevertheless, obvious paths exist which could strengthen the quality of the data, and hence confidence in the conclusions. A single plate scan, taking in a larger area around NGC 3311 at the same resolution and with more careful attention to stellar versus nonstellar image classification, would allow much stronger determinations of the troublesome background density σ_b, and in turn the radial and magnitude distributions of the globular clusters. Another step of major importance would be to set up a more direct and thorough magnitude calibration in selected areas around NGC 3311, most logically by CCD detector data. This latter approach would also allow a view of the central $\sim 1'$ of the galaxy, which could not be studied photographically. We are currently attempting to continue our investigation of the Hydra I system along these lines.

Without the help of Don Wells, through personal aid and his development of the appropriate image-reduction software at KPNO, this study would have been impossible. We are pleased to express our gratitude to him. This work was supported financially by the Natural Sciences and Engineering Research Council of Canada, through operating grants to W.E.H. and a summer assistantship to E.S.M.; and by the British Science and Engineering Research Council, through support of the Royal Observatory, Edinburgh. Finally, we are indebted to David Hanes and René Racine for numerous important comments and suggestions which improved the manuscript.

REFERENCES

Aaronson, M., Huchra, J., Mould, J., Schechter, P., and Tully, R. B. 1982, *Ap. J.*, **258**, 64.
Aaronson, M., Mould, J., Huchra, J., Sullivan, W. T., Schommer, R., and Bothun, G. 1980, *Ap. J.*, **239**, 12.
Boughn, S. P., Cheng, E. S., and Wilkinson, D. T. 1981, *Ap. J.* (*Letters*), **243**, L113.
de Vaucouleurs, G., and Buta, R. 1978, *A.J.*, **83**, 1383.
Forte, J. C., Martinez, R. E., and Muzzio, J. C. 1982, *A.J.*, **87**, 1465.
Forte, J. C., Strom, S. E., and Strom, K. M. 1981, *Ap. J.* (*Letters*), **245**, L9.
Hanes, D. A. 1977, *Mem. R.A.S.*, **84**, 45.
______. 1979, *M.N.R.A.S.*, **188**, 901.
______. 1982, invited paper at specialist session on the extragalactic distance scale, IAU General Assembly, August 1982, Patras.
Harris, W. E. 1976, *A.J.*, **81**, 1095.
______. 1981, *Ap. J.*, **251**, 497.
Harris, W. E., and Petrie, P. L. 1978, *Ap. J.*, **223**, 88.
Harris, W. E., and Racine, R. 1979, *Ann. Rev. Astr. Ap.*, **17**, 241 (HR).
Harris, W. E., and Smith, M. G. 1976, *Ap. J.*, **207**, 1036.
______. 1981, *A.J.*, **86**, 90.
Harris, W. E., and van den Bergh, S. 1981, *A.J.*, **86**, 1627.
Hewett, P. C., MacGillivray, H. T., and Dodd, R. D. 1981, *M.N.R.A.S.*, **195**, 613.
Jarvis, J. F., and Tyson, J. A. 1981, *A.J.*, **86**, 476.
Kron, R. 1980, *Ap. J. Suppl.*, **43**, 305.
MacGillivray, H. T., Martin, R., Pratt, N. M., Reddish, V. C., Seddon, H., Alexander, L. W. G., Walker, G. S., and Williams, P. R. 1976, *M.N.R.A.S.*, **176**, 265.
Mould, J. M., Aaronson, M., and Huchra, J. 1980, *Ap. J.*, **238**, 458.
Oemler, A. 1976, *Ap. J.*, **209**, 693.
Richter, O.-G., Materne, J., and Huchtmeier, W. K. 1982, *Astr. Ap.*, **111**, 193.
Sandage, A., and Tammann, G. A. 1974, *Ap. J.*, **194**, 559.
Sandage, A., and Visvanathan, N. 1978, *Ap. J.*, **223**, 707.
Smith, M. G., and Weedman, D. W. 1976, *Ap. J.*, **205**, 709 (Paper I).
Smyth, R. J. 1983, preprint.
Strom, S. E., Forte, J. C., Harris, W. E., Strom, K. M., Wells, D. C., and Smith, M. G. 1981, *Ap. J.*, **245**, 416.
Stryker, L. 1981, Ph.D. thesis, Yale University.
van den Bergh, S. 1977*a*, *Vistas Astr.*, **21**, 71.
______. 1977*b*, *Ap. J.*, **212**, 317.
Wells, D. 1980, Data Reduction and Analysis Report Series, No. 1., AUTOPHOT, Kitt Peak National Observatory.

William E. Harris: Dept. of Physics, McMaster University, Hamilton, Ont. L8S 4M1, Canada

Eric S. Myra: Dept. of Physics, University of Pennsylvania, Philadelphia, PA 19104

Malcolm G. Smith: Royal Observatory, Blackford Hill, Edinburgh EH9 3HJ, Scotland, UK